Int J Adv Manuf Technol (2015) 80:1721–1731
DOI 10.1007/s00170-015-7046-x

ORIGINAL ARTICLE

Integration strategy of on-machine measurement (OMM) and numerical control (NC) machining for the large thin-walled parts with surface correlative constraint

H. B. Liu[1] **· Y. Q. Wang**[1] **· Z. Y. Jia**[1] **· D. M. Guo**[1]

Received: 9 December 2014 / Accepted: 16 March 2015 / Published online: 25 April 2015

Abstract There is a kind of large thin-walled parts in aerospace industry, the machining target surface of which is tightly associated with another specific surface (named correlative surface). And it is always the primary machining objective. However, the preformed correlative surface is significantly different from its original design model due to large profile and thickness errors. Thus, part-referenced machining is necessary to ensure the correlative constraint accuracy. In this article, an integration strategy of OMM and NC machining for the large thin-walled parts with surface correlative constraint is systematically developed. Generally, the integration process consists of correlative constraint analysis, on-machine measurement, machining target surface redesign, and NC machining. Firstly, an isoplanar-based on-machine scanning method is presented for large surface profile information extraction. Then, a unified target surface redesign model is established according to surfaces accompanying relation analysis. Further, to compensate stress-induced monotonic structural deformation, a partitioned measuring and machining approach has been employed. Finally, the liquid rocket engine nozzle as a typical part was employed to verify the validation of the proposed strategy. Coolant channel machining experiments were conducted on a special dual-spindle machine tools. For a nozzle with machining area about 8 m^2, the correlative accuracy could be controlled in the range of ±0.1 mm. It has been proved that incorporating dimensional metrology feedback to machining process could consistently improve machining quality and efficiency of large thin-walled parts.

Keywords On-machine measurement · Large thin-walled parts · Surface correlative constraint · Surface redesign · Rocket nozzle

✉ H. B. Liu
hbliu@dlut.edu.cn

Y. Q. Wang
yqwang@dlut.edu.cn

Z. Y. Jia
jzyxy@dlut.edu.cn

D. M. Guo
guodm@dlut.edu.cn

[1] Key Laboratory for Precision and Non-traditional Machining Technology of Ministry of Education, Dalian University of Technology, Dalian 116024, China

Abbreviations

OMM	On-machine measurement
NC	Numerical control
MCP	Multi-cut process
RFQs	Radio-frequency quadrupoles
FCS	Fiducial calibration system
CMM	Coordinate measuring machine
CNC	Computer numerical control
1D	One-dimensional
2D	Two-dimensional
3D	Three-dimensional
CAD	Computer aided design
API	Application programming interface
CL	Cutter location
PC	Personal computer
VC++	Visual C++

1 Introduction

1.1 Background

As is well known, large thin-walled parts with high specific strength and high specific stiffness play an important role in the aerospace equipment (such as aircraft, rocket, and artificial satellite), which are generally the main functional components undertaking the tasks of energy transmission, load bearing, or action response in some extreme working conditions (e.g., hundreds of tons of pressure, thousands of degrees of ambient temperature or over 5g acceleration). Therefore, the mechanical uniformity, the structural integrity, and the accuracy consistency of these machined parts have a significant impact on equipment whole working performance.

One typical example is the liquid rocket engine nozzle, shown in Fig. 1. Nozzle is used to convert combustion thermal energy into launching thrust force. Nozzle is a large regeneratively cooled reusable structure, which is formed through brazing two complex rotary thin-walled sheet metals together, a liner and a jacket. Hundreds of the coolant channels should be machined on the outside surface of the liner. The hot gas wall thickness (i.e., channel remaining wall thickness) must be precisely controlled relative to the liner inside surface. Otherwise, the cooling effect would be very poor.

Another example is the rocket fuel tank. Thousands of triangular or quadrilateral grids densely distributed on the inner wall for weight reduction should be machined. In order to obtain reliable resistance capability of on the impact of strong dynamic launching load, the machined grid remaining wall thickness with minimal variability is necessary.

The machining of large thin components as monolithic structures has largely replaced sheet metal assembly operations [20]. Considering the manufacturing cost and efficiency, the sacrificial structure preforms created in the ways of spinning, welding, or stretch forming have been widely employed, instead of direct machining the part from a huge solid [21]. However, the forming error is often much larger than the finished tolerance. As a result, to ensure the machining, accuracy has become a challenge.

Generally, the main machining characteristics of the large thin-walled part are

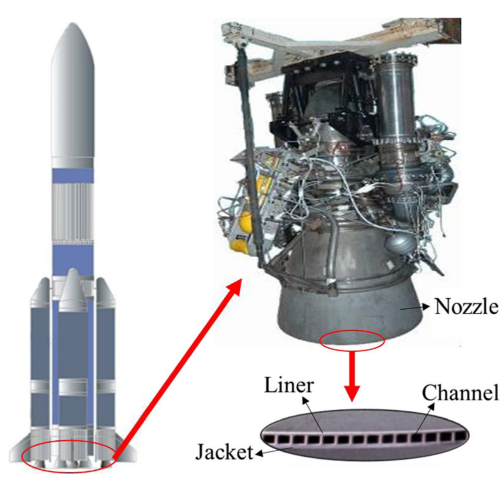

Fig. 1 Liquid rocket engine nozzle

- *Tight surface correlative constraint*: the machined target surface is tightly associated with a specific surface (named correlative surface) of the part itself or other parts (e.g., precision surface assembly). And it is always the primary machining objective of the large thin-walled parts.
- *Part-referenced machining*: the formed correlative surface is significantly different from its original design model due to the large profile or thickness errors. Thus, the position and posture of the machined target surface should vary accurately along with the actual correlative surface. Thus, the machining needs part referencing.

For these types of large thin-walled parts, some machining issues will outstand significantly (I) the criterion of the conformity of a machined part to its theoretical design model is weakened [10]; (II) the long-range accuracy and the thermal environment dictate the minimum capable tolerances, and these factors therefore impose limitations on part size [20, 23]; and (III) the simulation-based deformation compensation is overworked due to the large size, the complex geometric boundary condition, and the loads distribution (such as clamping force, inherent residual stress) [1, 24].

1.2 Literature review

In recent decades, improving the machining accuracy of low rigidity parts has been attracting a great number of researches. Active methodologies mainly include simulation-based prediction and compensation, OMM-based dimension closed-loop control.

For thin-walled part, such as the cantilever-type parts and the plate-type parts, lots of researches focus on the simulation-based numerical prediction of force-induced local elastic deformation [2, 4, 18, 19] and the stress-induced overall deformation [3, 16, 22], respectively. Using the deformation simulation results, the toolpaths and the cutter localizations can be compensated point-by-point. Consequently, the machining accuracy can be improved. However, for large thin-walled part, less concerned the coupled effect of the two kinds of deformations. Otherwise, it would result in severe distortion because of the weakened rigidity and the release of residual stress. Moreover, to identify the complex geometric and the clamping force boundary conditions precisely is another thorny problem.

With the continual development of modern manufacturing technology, incorporating dimension metrology feedback to the machining process has necessitated a critical evolution activity to consistently improve part quality and manufacturing efficiency [5, 6, 9, 17]. Using OMM, the part geometry can be measured by replacing cutter using probe at its machining setup. Thus, it needs to integrate part measurement into machine. The machine tools will act as a material removal device and a measurement device simultaneously. The integration can not only determine the part state on fixtures in machine workspace but also direct feedback part information to processing.

Process-intermittent gauging by on-machine probing can detect errors due to the cutting action, such as part deflection [8]. For the multi-cut process (MCP), the trend of the cutting deviation is estimated using the probing data, then the multi-tool path is modified using the discrete compensation vectors computed according to the cutting compliance model. On the base of 3-axis tool path iterative compensation, the cutting force-induced errors of flexible thin-walled parts were adaptively decreased based on OMM by the modifying 5-axis flank milling toolpath [11]. In order to obtain a precision assemble of radio-frequency quadrupoles (RFQs) cavity, the measured values were fed back to offset the final cut depths and achieve the required vane-tips machining accuracy [14]. In radome grinding, the actual inner contour surface of semi-finishing parts obtained on machine was employed to calculate the target surface under the requirements of precision electromagnetic wave transparent [10, 12]. Fiducial calibration system (FCS) was proposed for the first time, which could provide a method that allows for the accuracy of a coordinate measuring machine (CMM) to be transferred to the shop floor [20, 25]. This technique can be extended to allow small machines to manufacture large components and is also applicable in high volume manufacturing environments. However, the ability to compensate the deformation errors is limited by the ability to locate the fiducials.

The benefits of OMM-based machining strategy include no accurate machines in a tightly controlled thermal environment is required, no precision part alignment with machine axes is required, and no explicit knowledge of part structural deformation is required. However, bringing together these two previously decoupled operations, measurement and machining, has revealed a number of additional issues that are directly related to the integration into a common platform or manufacturing system, including data communication, information fusion, coordinate transition, and accuracy compatibility [8, 13, 17, 25].

1.3 Research objective

The objective of this article is to develop an efficient and reliable manufacturing strategy by integrating OMM and NC machining for the large thin-walled parts with surface correlative constraint. The paper is organized as: the principle of integration strategy is introduced in section 2; large surface on-machine scanning and target surface redesign and machining are described in detail in section 3 and section 4, respectively; finally, taking the rocket engine nozzle as a typical workpiece to verify the validation of the proposed approach experimentally is highlighted in section 5.

2 Integration strategy of OMM and NC machining

For the large thin-walled parts with surface correlative constraint, the correlative surface is the machining reference, and the target surface should vary passively. In other words, the target surface can only be determined on the basis of the correlative surface and the surface correlative constraint relation. Generally, the surface correlative constraint relation is given before machining, e.g., the distributed thickness. However, the actual correlative surface is always unknown. One reason is that the profile error of the preformed part is mostly larger than the designed tolerance after sheet metal preforming and part clamping. The other is the significant structural deformation induced by inherent stress relaxation and rebalance during long-term machining. As a result, in order to guarantee the required surface correlative constraint relation accurately, the actual correlative surface needs to be determined on machine, and the target surface can further be re-generated (named surface redesign in this article). Thence, the process is indeed an integration of OMM and NC machining.

2.1 Definition of the correlative accuracy

According to the above analysis, there is a strict spatial geometric relation between the target surface $\boldsymbol{S}^T$ and the correlative surface $\boldsymbol{S}^C$. In order to describe the correlative constraint relation exactly, a novel correlative accuracy should be defined. Firstly, a correlative distance should be defined as the distance between the point on $\boldsymbol{S}^C$ and the mapping point on $\boldsymbol{S}^T$ along a constraint direction. Then, a correlative accuracy is defined as a deviation of the actual correlative distance relative to the required.

Without loss of generality, both $\boldsymbol{S}^T$ and $\boldsymbol{S}^C$ are assumed to be smooth and regular three-dimensional (3D) Euclidean space $\mathbb{R}^3$, $\boldsymbol{S}^T(u^T,v^T)\in\boldsymbol{R}^3$, $\boldsymbol{S}^C(u^C,v^C)\in\boldsymbol{R}^3$, (u^T,v^T), and (u^C,v^C) are surface parameters of $\boldsymbol{S}^T$ and $\boldsymbol{S}^C$, respectively. The correlative distance $\mathbf{d}_{T\text{-}C}$ is a directional spatial distance, shown in Fig. 2. Thus, the deviation δ can be formulated mathematically as

$$\delta = \left\{\|\mathbf{d}_{T-C}\|_2 - d_0\right\} = \min_{(u^T,v^T)} (\mathbf{p}-\mathbf{q})\cdot\mathbf{n}^{\mathbf{q}} - d_0 \tag{1}$$

where $\mathbf{q}$ is the point on $\boldsymbol{S}^C$, $\mathbf{q}\in S^C$; $\mathbf{p}$ is the mapping point on $\boldsymbol{S}^T$, $\mathbf{p}\in S^T$; d_0 is the designed correlative distance at the point $\mathbf{q}$; and $\mathbf{n}^{\mathbf{q}}$ is the correlative direction of point $\mathbf{q}$, which is generally consistent with the normal vector $\mathbf{N}^{\mathbf{q}}$ of point $\mathbf{q}$. Actually, the point $\mathbf{p}$ is the spatial closest point relative to the point $\mathbf{q}$ along the direction $\mathbf{n}^{\mathbf{q}}$, which could be calculated iteratively. It can be seen that the correlative accuracy is essentially a relative position accuracy.

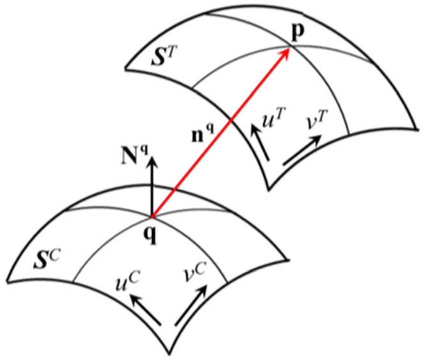

Fig. 2 The correlative relations of $\boldsymbol{S}^T$ and $\boldsymbol{S}^C$

2.2 The integration process description

The integration process of OMM and NC machining of the large thin-walled parts is shown in Fig. 3, which is mainly composed of four phases, including correlative constraint analysis, on-machine measurement, target surface redesign, and NC machining, respectively, detailed as follows:

- *Correlative constraint analysis*: generally, for a given large thin-walled part, three typical surfaces and one relation should be firstly identified and determined according to part machining requirements and its clamping configuration. The three typical surfaces are named the measured surface, the correlative surface, and the target surface, respectively. One relation is the surface constraint relation between the target surface and the correlative surface.
- *On-machine measurement*: one critical task is the profile information on-machine extraction of the large and complex measured surface. To balance measuring speed and accuracy is a difficult issue. The stepwise decomposition strategy from the measured surface to the point set would be a practical and efficient method.
- *Target surface redesign*: the target surface should be redesigned using the on-machine measured results under the condition of correlative constraint. To formulate the constraint relations and to reconstruct the correlative surface are two key issues.
- *NC machining*: during this phase, the redesigned target surface is used to plan the CLs under a certain conditions of clamping. It should be noted that the monolithic structural deformation induced by stress relaxation is particularly prominent, which cannot be ignored. As a result, if the initial CLs were still being executed, there would be large dimension errors for the left machining area.

Fig. 3 Flow chart of the integration process

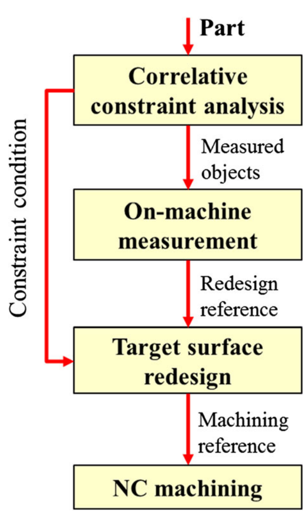

3 Large surface on-machine scanning

The isoplanar-based on-machine scanning method is adopted for the large surface [15], shown in Fig. 4. It can provide an opportunity to simplify measuring movement from 3D space to 2D space for both noncontact and contact sensors. Three orthogonal Cartesian systems are firstly defined, including the machine coordinate system $\{\boldsymbol{C}_M$: $\boldsymbol{O}_M$-$\boldsymbol{X}_M\boldsymbol{Y}_M\boldsymbol{Z}_M\}$, sensor coordinate system $\{\boldsymbol{C}_S$: $\boldsymbol{O}_S$-$\boldsymbol{X}_S\boldsymbol{Y}_S\boldsymbol{Z}_S\}$, and part coordinate system $\{\boldsymbol{C}_P$: $\boldsymbol{O}_P$-$\boldsymbol{X}_P\boldsymbol{Y}_P\boldsymbol{Z}_P\}$. The measured surface is discretized by a set of infinite parallel planes, named digital plane. In general, the selected digital planes coincide with a machine coordinate plane to simplify the scanning movement. In scanning, the probe is driven from one control point to the next control point along linear control path in digital planes. At the same time, a wealth of coordinate information will be extracted by sampling system at the designed frequency. Thus, the part geometric information can be described in $\boldsymbol{C}_M$.

3.1 Modeling the on-machine scanning

Surface information extraction is essentially a coordinate transformation process from $\boldsymbol{C}_S$ to $\boldsymbol{C}_M$. Generally, the coordinate information of each point consists of two components, 3D sensing information and the corresponding machine coordinates, both of which are picked up in one sampling period. The basic model of coordinate information extraction is expressed in $\boldsymbol{C}_M$ as

$$\begin{cases} [\mathbf{p}_M, 1]^T = \mathbf{T}_M^S \cdot [\mathbf{p}_S, 1]^T \\ \mathbf{T}_M^S = \begin{bmatrix} \mathbf{R}_M^S & \mathbf{P}_M^S \\ \mathbf{0} & 1 \end{bmatrix} \end{cases} \qquad (2)$$

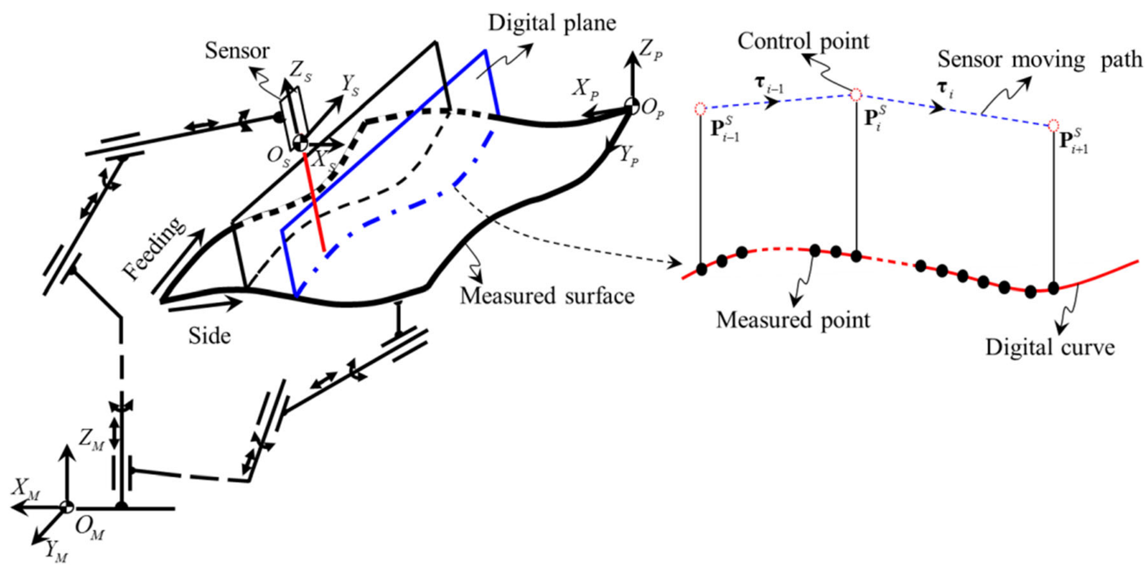

Fig. 4 The isoplanar-based on-machine scanning

where $\mathbf{p}_M$ and $\mathbf{p}_S$ denote the coordinate in $\boldsymbol{C}_M$ and sensing information in $\boldsymbol{C}_S$, respectively. $\mathbf{T}_M^S$, $\mathbf{R}_M^S$, and $\mathbf{P}_M^S$ denote the comprehensive transformation matrix, the rotational transformation matrix, and the translation transformation matrix from $\boldsymbol{C}_S$ to $\boldsymbol{C}_M$, respectively. The $\mathbf{R}_M^S$ describes the posture variation of the $\boldsymbol{C}_S$ with respect to its initial state, which can be represented by the roll angle α, the pitch angle β and the yaw angle γ. And these angles would be estimated according to the machine angle coordinates of the current sampling points. Moreover, the $\mathbf{P}_M^S$ is composed of two parts, one is the origin deviation of the $\boldsymbol{C}_S$ from the $\boldsymbol{C}_M$ when the machine tools locates at the initial origin, and the other is the machine translation coordinates of the current sampling points. The sampling coordinate extraction process is illustrated in Fig. 5.

The $\mathbf{R}_M^S$ and the $\mathbf{P}_M^S$ are formulated as,

$$\mathbf{R}_M^S = \begin{bmatrix} \cos\gamma\cos\beta & \cos\gamma\sin\beta\sin\alpha - \sin\gamma\cos\alpha & \cos\gamma\sin\beta\cos\beta + \sin\gamma\sin\alpha \\ \sin\gamma\cos\beta & \sin\gamma\sin\beta\sin\alpha + \cos\gamma\cos\alpha & \sin\gamma\sin\beta\cos\alpha - \cos\gamma\sin\alpha \\ -\sin\beta & \cos\beta\sin\alpha & \cos\beta\cos\alpha \end{bmatrix} \quad (3-a)$$

$$\begin{cases} \mathbf{P}_M^S = \boldsymbol{\varepsilon}_M^S + \mathbf{t}_M^S \\ \boldsymbol{\varepsilon}_M^S = \left[\varepsilon_x, \varepsilon_y, \varepsilon_z\right]^T \\ \mathbf{t}_M^S = \left[t_x, t_y, t_z\right]^T \end{cases} \quad (3-b)$$

where $\boldsymbol{\varepsilon}_M^S$ and $\mathbf{t}_M^S$ are the origin deviation vector and the machine translation vector, respectively; ε_x, ε_y, and ε_z are the origin deviation components; t_x, t_y, and t_z are the machine translation components. The origin deviations can be estimated through sensor position calibration using an artificial tool. At this time, the axes of $\boldsymbol{C}_S$ are generally selected to be consistent with the axes of $\boldsymbol{C}_M$ for the origin deviations calibration, thus the $\mathbf{R}_M^S$ is a unit matrix.

In engineering, a directional scanning approach is sometimes adopted to obtain a higher scanning speed. Thus, the $\mathbf{R}_M^S$ is generally a constant matrix.

In $\boldsymbol{C}_S$, for different types of sensors, the $\mathbf{p}_S$ can be expressed as follows:

$$\mathbf{p}_S = \begin{cases} [0, 0, d_S]^T & \text{for 1D sensor} \\ [0, d_\theta \sin\theta, d_\theta \cos\theta]^T & \text{for 2D sensor} \\ \left[e_S^x, e_S^y, e_S^z\right]^T & \text{for 3D sensor} \end{cases} \quad (4)$$

where d_S is the detecting distance for one-dimensional (1D) sensor, e.g., point laser sensor; d_θ is the detecting distance at the viewing angle θ in the viewing field for 2D sensor, e.g., line laser sensor; and the direction the θ is defined according to the right-hand rule; e_S^x, e_S^y, and e_S^z are the deviations along X_S-axis, Y_S-axis, and Z_S-axis, respectively, for 3D sensor, e.g., 3D contact scanning probe.

The scanning motion is constrained within the digital planes, and the probe is driven continuously from the current control point $\mathbf{P}_i^S$ to the next control point $\mathbf{T}_{i+1}^S$ at a scanning speed F_S along the i_{th} scanning direction $\boldsymbol{\tau}_i$.

$$\mathbf{P}_{i+1}^S = \mathbf{P}_i^S + \lambda_i \boldsymbol{\tau}_i \quad (5)$$

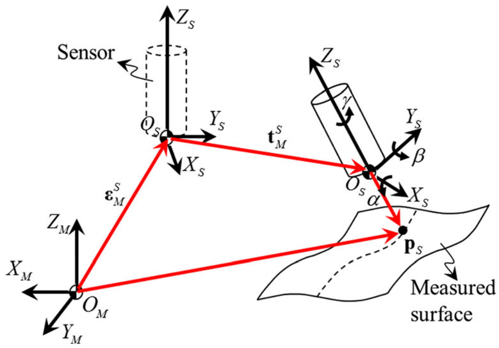

Fig. 5 The illustration of coordinate extraction

where λ_i denotes the i_{th} feeding control step along the scanning direction $\boldsymbol{\tau}_i$. It can be seen that the scanning direction and the control step are two critical factors influenced sampling efficiency and accuracy for surface measurement.

Further, the probe sensing frequency is much higher than data communicating frequency of sampling system. Therefore, it is necessary to deal with the frequency mismatch between data collecting and storing, which may result in measuring information loss. Frequency-sharing approach can be adopted using multi-thread data storing mechanism. One thread is used to set up a high frequency data channel from probe to memory in hardware layer. In the other thread, the information will be picked up from memory to PC at a lower frequency in software layer.

3.2 Sensor location calculation

If the CAD model of the measured surface can be used to assist the surface scanning, i.e., named model-known, it is crucial to determine the locations of the digitized lines extracted from the measured surface CAD model. Firstly, the sensing accessibility of the selected scanning probe should be analyzed in the collision-free measurable space, which can be defined a geometric coupling of two spaces of probe, the kinematic configuration space and the visual space. The visual space of laser sensor can be approximated by cone and cylinder for contact probe. The location determination is generally composed of three parts, intersecting calculation between spatial digitized planes and CAD model using parametric grid discretization method or tracing method, and feeding steps and side steps calculation using the minimizing local curvature method.

As contrast, for model-unknown surface scanning [15], the measured coordinate points will be utilized to predict the feeding control step λ_1, the side control step λ_2, and the scanning direction $\boldsymbol{\tau}$. Two moving reference windows W_1 with width of N_1 and W_2 with width of N_2 should be built as the bases in feeding direction and side direction, respectively. And a hybrid extrapolation approach combined curvature extrapolation mode and tangent extrapolation mode can be employed to predict the feeding control step and the scanning direction adaptively in each digital plane. In scanning, the reference W_1 should be updated dynamically by the fresh measured points. Similarly, the side step can be predicted using the measured digital curves in reference W_2. In this way, the measured surface can be felt precisely by the sensor step by step.

4 Target surface redesign and machining

4.1 Surfaces accompanying relation

Parametric surfaces S and S^* are two smooth and regular surfaces in $\mathbb{R}^3$. If there is a point-to-point mapping between the two surfaces, a surface-accompanying relation has been established [7]. Without loss of generality, S is the defined reference surface, and S^* is the accompanying surface. In order to formulate the surfaces accompanying relation, the first-order frame $\{\mathbf{e}_i, i=1,2,3\}$ should be established on the surface S using the Schmidt orthogonalizing technique, which is a unit orthonormal frame. The parametric expression of S is $\mathbf{r}=\mathbf{r}(u,v)=[x(u,v),y(u,v),z(u,v)]^T$, (u,v) is the parameter field of S. Thus, the first-order frame is formulated as

$$\begin{bmatrix}\mathbf{e}_1\\ \mathbf{e}_2\\ \mathbf{e}_3\end{bmatrix} = \begin{bmatrix} 1/\sqrt{E} & 0 & 0\\ \dfrac{-F}{\sqrt{E(EG-F^2)}} & \dfrac{\sqrt{E}}{\sqrt{EG-F^2}} & 0\\ 0 & 0 & 1\end{bmatrix}\cdot\begin{bmatrix}\mathbf{r}_u\\ \mathbf{r}_v\\ \mathbf{n}\end{bmatrix} \tag{6}$$

where E, F, and G are the basic coefficients of the surface first fundamental form; $\mathbf{r}_u$ and $\mathbf{r}_v$ denote the tangential vector along u -direction and v -direction, respectively; $\mathbf{n} = (\mathbf{r}_u \times \mathbf{r}_v)\,/\,\sqrt{EG}$ is the unit normal vector; $\{\mathbf{r}_u, \mathbf{r}_v, \mathbf{n}\}$ is the surface natural frame field or Gauss frame field. According to Eq. (6), $\mathbf{e}_3$ is consistent with $\mathbf{n}$. And if the established parameter field (u,v) is orthogonal, $F\equiv 0$.

Therefore, the accompanying surface S^* is formulated as

$$\mathbf{r}^* = \mathbf{r} + \sum_{i=1}^{3} \varsigma_i(u,v)\mathbf{e}_i \tag{7}$$

where $\mathbf{r}^*$ is the parametric expression of S^*, and $\varsigma_i (i=1, 2,3)$ is the mapping components along the local coordinate axis $\mathbf{e}_i$.

If the mapping points on S^* locates in the normal direction of S, the normal accompanying relation will be established, and the surface S^* can be called normal accompanying surface. Thus, the mapping components are $\varsigma_1=0$, $\varsigma_2=0$, and $\varsigma_3=h(u,v)$; $h(u,v)$ is normal mapping function or thickness distribution function. And if h is constant, the accompanying relation between the two surfaces can be recognized as the isometric accompanying.

4.2 Modeling of surface redesign

According to correlative constraint analysis, three typical surfaces are generally picked up for a large thin-walled part, the measured surface $\boldsymbol{S}^M$, the correlative surface $\boldsymbol{S}^C$, and the target surface $\boldsymbol{S}^T$. Meanwhile, four frames are also defined, including the global frame $\{\boldsymbol{C}_0: O_0, e_i^0\ (i=1,2,3)\}$ connected with machine, the measuring frame $\{\boldsymbol{C}_1: O_1, e_i^1\ (i=1,2,3)\}$ connected with $\boldsymbol{S}^M$, the correlative frame $\{\boldsymbol{C}_2: O_2, e_i^2\ (i=1,2,3)\}$ connected with $\boldsymbol{S}^C$, and the target frame $\{\boldsymbol{C}_3: O_3, e_i^3\ (i=1,2,3)\}$ connected with $\boldsymbol{S}^T$. The $\boldsymbol{C}_0$ is the same as the $\boldsymbol{C}_\mathrm{M}$. The latter three frames are surface local first-order frames. The spatial configuration relation of the three surfaces is shown in Fig. 6.

Actually, there are two surfaces accompanying relations, one between the $\boldsymbol{S}^M$ and the $\boldsymbol{S}^C$, the other between the $\boldsymbol{S}^C$ and the $\boldsymbol{S}^T$. Therefore, the target surface $\boldsymbol{S}^T$ can be described directly in $\boldsymbol{C}_0$ using the basic surfaces accompanying model Eq.(7) in section 4.1. The parametric model is as follows:

$$\mathbf{r}_0^3 = \mathbf{r}_0^1 + \mathbf{r}_1^2 + \mathbf{r}_2^3 = \mathbf{r}_0^1 + \sum_{i=1}^{3} a_i \mathbf{e}_i^1 + \sum_{i=1}^{3} b_i \mathbf{e}_i^2$$
$$= \mathbf{r}_0^1 + \sum_{i=1}^{3}\left(a_i + \sum_{j=1}^{3} b_j c_j^i\right)\mathbf{e}_i^1 \qquad (8)$$

where $\mathbf{r}_i^j(i,j=1,2,3)$ is the translational vector of the j_{th} frame origin relative to the i_{th} frame; $\mathbf{e}_i^j$ is the i_{th} frame axis of the j_{th} frame; a_i and b_i are the translational components along the frame axis $\mathbf{e}_i^1$ and $\mathbf{e}_i^2$, respectively; c_i^j is rotational component of the j_{th} frame axis of $\boldsymbol{C}_2$ relative to the i_{th} frame axis of $\boldsymbol{C}_1$.

Further, the Eq.(8) is converted using vector-matrix formulation as follows:

$$\mathbf{r}_0^3 = \mathbf{r}_0^1 + \left(\mathbf{T}_1^2 + \mathbf{T}_2^3 \cdot \mathbf{R}_1^{2\,T}\right) \cdot \mathbf{E}^{1\,T} \qquad (9)$$

where $\mathbf{E}^1$ denotes axis vectors of $\boldsymbol{C}_1$. $\mathbf{T}_1^2$ and $\mathbf{R}_1^2$ are the translation matrix and the rotational matrix of $\boldsymbol{C}_2$ relative to $\boldsymbol{C}_1$, respectively, which denote the indirect correlative constraint array. $\mathbf{T}_2^3$ is the translation matrix of $\boldsymbol{C}_3$ relative to $\boldsymbol{C}_2$ which denotes the direct correlative constraint array. The $\mathbf{r}_0^1$ can be obtained by OMM according to section 3. $\mathbf{E}^1$ will be calculated using the measured $\mathbf{r}_0^1$.

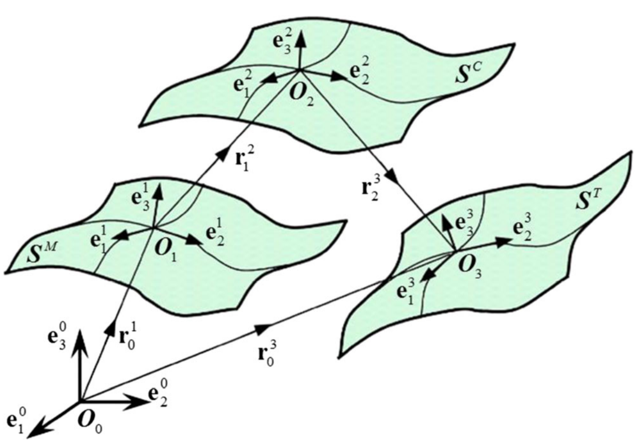

Fig. 6 Surfaces spatial configuration relations

Two spatial cases should be discussed for target surface generation

(1) Normal accompanying relation

Actually, the preformed profile error and the thickness error are still very small relative to the size of the large thin-walled parts. Thus, the spatial relations between the $\boldsymbol{S}^M$ and the $\boldsymbol{S}^C$, and between the $\boldsymbol{S}^C$ and the $\boldsymbol{S}^T$, can be approximated as normal accompanying relation. As a result, the translation matrices $\mathbf{T}_1^2$ and $\mathbf{T}_2^3$ are $\mathbf{T}_1^2=[0,0,h_1^2]^T$ and $\mathbf{T}_2^3=[0,0,h_2^3]^T$. h_1^2 and h_2^3 are the thickness distribution functions of the surface $\boldsymbol{S}^C$ relative to the surface $\boldsymbol{S}^M$ and the surface $\boldsymbol{S}^T$ relative to the surface $\boldsymbol{S}^C$, respectively. The h_2^3 is the required correlative distance. And the h_1^2 needs to be determined on machine. And the rotational matrix $\mathbf{R}_1^2$ can be approximated using the surface design model.

(2) The surface $\boldsymbol{S}^M$ and the surface $\boldsymbol{S}^C$ are the same

Thus, the surface $\boldsymbol{S}^C$ can be on-machine measured directly. And, the target surface model should be modified according to Eq.(9) as

$$\mathbf{r}_0^3 = \mathbf{r}_0^2 + \mathbf{T}_2^3 \cdot \mathbf{E}^{1\,T} \qquad (10)$$

where $\mathbf{r}_0^2$ is the parametric expression of the $\boldsymbol{S}^C$ in $\boldsymbol{C}_0$.

4.3 Monolithic structural deformation partitioned compensation

For the large thin-walled parts, the material removal amount is very large (70~90 %), and the machining time is long (dozens of days), thus how to compensate the monolithic structural deformation induced by the inherent stress relaxation is a challenging work. It should be noted that this deforming process is very slow. So, a partitioned compensation strategy may supply a flexible and efficient solution for this quasi-static deformation compensation. It is an intermittent process because the activities of measurement and machining will be carried out by turn.

The deformation partitioned compensation approach is illustrated in Fig. 7, which is mainly composed of two stages, (I) surface partitioned and (II) partitioned machining. In stage I, the unfolded surface is divided into several machining subregions $\{\Pi_i, i=1,\ldots,N\}$, the machining subregion boundaries are denoted by two-dot chain lines. The partition size is a critical factor, which will affect compensation accuracy and machining efficiency directly. Thus, the following basic principles should be followed in partition planning; one, the larger deformation gradient, the smaller of the sub-regions, and vice versa, e.g., in large curvature area; two, the compensation proportion is generally 50~60 % of the correlative dimension tolerance. At present, FEM-based deformation analysis and engineering experience can be combined to assist partition planning, even though to build a unified and accurate model is almost impossible for large thin-walled part. In stage II, the subregion will be machined using the developed integration strategy of OMM and NC machining. In each machining subregion, four works needs to be done, the surface $\boldsymbol{S}^M$ on-machine measuring, the surface $\boldsymbol{S}^T$ redesign using the developed model, CLs calculation and NC machining implementation. After one subregion, the four works will be repeated in the next subregion until the whole part machining is completed.

5 Experimental verification using rocket engine nozzle

Liquid rocket engine nozzle as a typical application was employed to verify the validation of the developed measurement-machining integrated manufacturing strategy. Coolant channels machining on the liner (a large thin-wall rotary shell) is its critical machining problem.

5.1 Structure characteristics and machining requirements of nozzle

As shown in Fig. 8a, the main geometric parameters of nozzle liner are diameter 1~2 m, height 1~2 m, sheet thickness 4~6 mm, and hundreds of channels on the outer surface of the liner, respectively. The theoretical nozzle profile is complex rotary surface, bell contour or expansion-deflection contour (E-D contour). And the hot gas wall thickness distribution is given before machining, uniform, or variation.

The surfaces correlative relation of nozzle is shown in Fig. 8b. There are three typical surfaces, the outer surface, the inner surface, and the channel bottom surface. The inner surface is the correlative surface, and the channel bottom surface is the target surface. And the remaining wall thickness between the channel bottom surface and the liner inner surface must be ensured precisely, which is the crucial machining quality index. In this sense, the correlative constraint relation has been established.

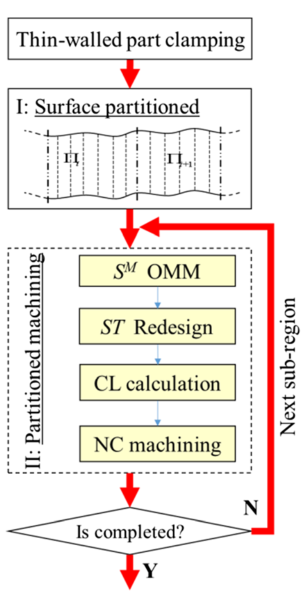

Fig. 7 The deformation partitioned compensation strategy

5.2 Coolant channel machining process and experiments

In order to guarantee the channel remaining wall thickness accuracy, the liner inner surface (as the correlative surface) needs to be determined on machine, and the channel bottom surface can be then redesigned according to the required remaining wall thickness function. From nozzle machining experiments, the stress-induced monolithic deformation is obviously dominated relative to the local elastic deformation induced by cutting force. The rotary shell with certain load resisting capacity may be the main reason. Therefore, to compensate the monolithic structural deformation, the nozzle surface was divided into eight machining subregions non-uniformly along the circumferential direction. The partition angles are 90°, 90°, 45°, 45°, 30°, 30°, 15°, and 15°, respectively. The coolant channel digital machining process on the nozzle liner is illustrated in Fig. 9.

A special dual-spindle CNC machine for nozzle channel symmetrical machining has been developed, shown in Fig. 9a. The positioning accuracy of the four linear servo axes is 0.005 mm in 800-mm horizontal travel and 0.007 mm in 1800-mm vertical travel, respectively. As for the rotary servo axis, the positioning accuracy is less than 5”. Further, the nozzle digital machining system was also built using the MICROSOFT VC++6.0 and the PC-based open application programming interface (API) functions. Therefore, the customized functions, such as on-machining laser measurement, surface redesign, and channel NC machining, can be realized according to the communication between application layer and the bottom real-time layer.

The nozzle coolant channel machining process is detailed as follows:

> Step 1, the preformed nozzle clamping. An inner surface supporting based clamping method was designed in Fig. 9b. The supporting surface of fixture mold is consistent with the theoretical inner surface. The nozzle

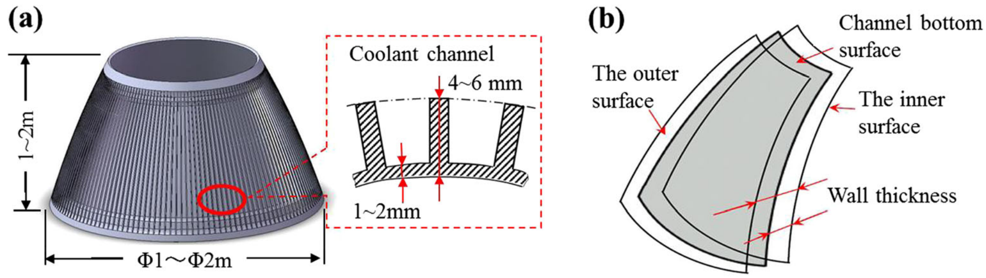

Fig. 8 Model of nozzle liner. **a** Geometric features and **b** surfaces correlative relation

clamping was conducted on a large NC press machine. The pressure was adjusted numerically. The clamping system rigidity would be improved through increasing supporting area and controlling circumferential stretching stress due to structure expansion. In such clamping condition, the correlative surface is completely invisible. As a result, two geometric features need to be measured on machine, the wall thickness and the outer surface.

Step 2, wall thickness ultrasonic measurement. The PANAMETRICS ultrasonic probe was used to determine the wall thickness distribution point by point along the nozzle generatrix. The coolant was selected as the coupling. The wall thickness detecting accuracy can be less than 0.01 mm after error compensation. The wall thickness distribution of one nozzle is shown in Fig. 10a. It can be seen that the nozzle is welded using three pieces of sheet metal, and the most volatile is the welded area. The wall thickness error is larger than 0.5 mm.

Step 3, outer surface dual-laser scanning. The isoplanar-based laser directional scanning method was used to extract nozzle outer surface information shown in Fig. 9c. Two MICRO-EPSILON ILD laser displacement sensors were employed. Thus, a dual-sensor symmetrical scanning system was established. The scanning procedure was programed using macro-instructions. The main laser scanning parameters were scanning speed 4~8 m/min and sampling frequency 125 Hz. The measured nozzle outer surface is shown in Fig. 10b. The number of measured points is more than 50,000. The laser inclination error should be compensated. Finally, the nozzle measurement accuracy can reach 0.03 mm.

Step 4, coolant channel bottom surface redesign. Using Eq.(9), the nozzle channel bottom surface was redesigned under the correlative constraint condition. First, the point cloud data of the outer surface was pre-processed, including noise removing, fairing, and data reduction. Second, the liner inner surface was calculated using the measured wall thickness and outer profile, as the machining datum. Then, the channel bottom surface was generated according to the designed remaining wall thickness function, a quarter of which is shown in Fig. 10c.

Step 5, coolant channel milling. An efficient channel milling approach was developed by a combination of a disk-type mill and an end mill. The former cutter was used to machine the main part of coolant channel, and the channel-end clearing was subsequently implemented using the latter cutter. Meanwhile, the partitioned machining strategy was adopted. According to the finite element analysis and machining experiences, the nozzle surface was uniformly divided into five regions. Thus, step 3 and step 4 should be repeated five times for one part. The diameter and the cutting teeth of the disk-type mill are 160 mm and 20, respectively. And the corresponding parameters of the end mill are 3 mm and 3, respectively. The

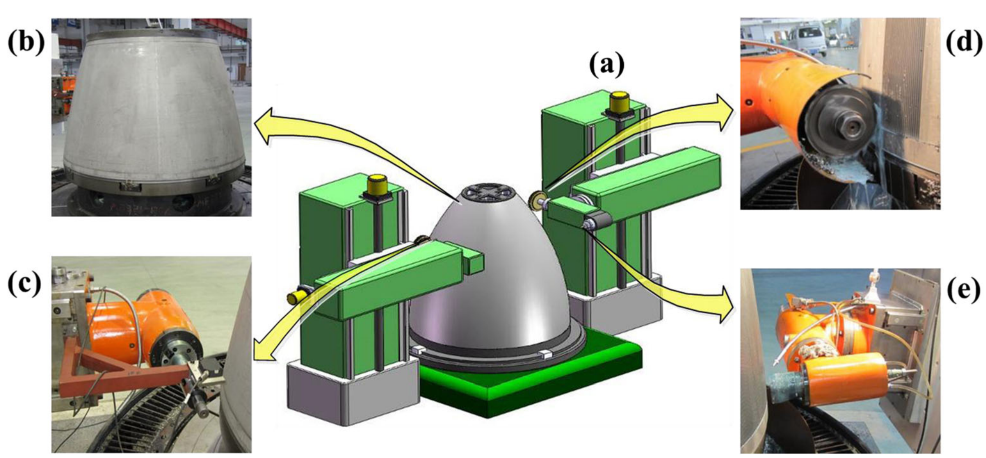

Fig. 9 Nozzle coolant channel digital machining. **a** special dual-spindle CNC machine, **b** nozzle clamping, **c** outer surface on-machine measurement, **d** disk-type milling, and **e** channel-end clearing

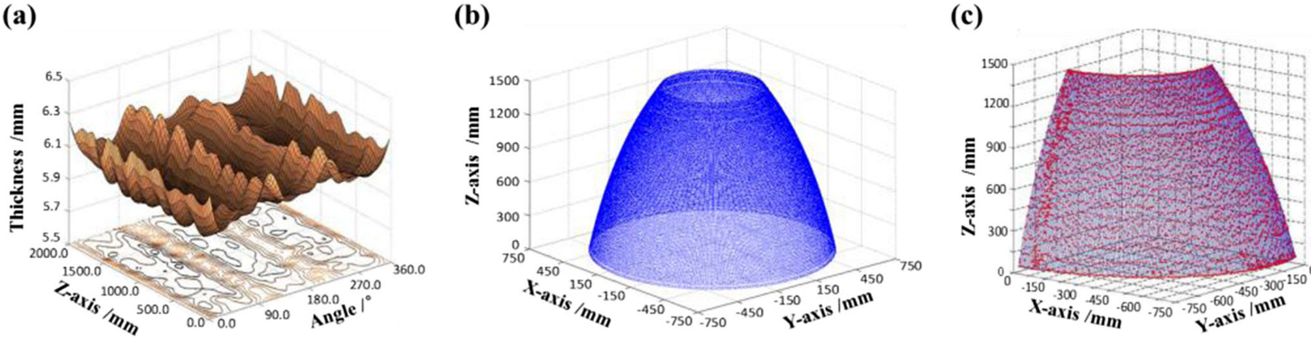

Fig. 10 Nozzle target surface redesign process. **a** Wall thickness distribution, **b** nozzle outer surface, and **c** CLs (denoted by *red points*) of a partitioned channel bottom surface

cutting speed is set about 50 m/min. The disk-type milling and the end milling were shown in Fig. 9d, e, respectively. At the same time, in each partition, the structure deformation was compensated through querying compensation table using macro function.

Step 6, correlative accuracy testing. The machined nozzle was taken off from the fixture mold shown in Fig. 11. The remaining wall thickness was tested manually using a pliers-type gauge. For a nozzle with machining area about 8 m^2, the final correlative accuracy achieved ±0.1 mm.

6 Conclusions

In this article, an integration strategy of OMM and NC machining for the large thin-walled parts with surface correlative constraint has been presented.

(I) The main machining characteristics of the large thin-walled parts are tight surface correlative constraint and part-referenced machining, the former is the primary machining requirement. Thus, the final machined target surface is significantly different from the original design model, personalized machining for each part.

Fig. 11 The machined rocket nozzle

(II) The integrated manufacturing process is mainly composed of on-machine surface scanning, target surface redesign, partitioned measurement, and machining, all of which should be conducted on a special digital system.

(III) The liquid rocket engine nozzle was used to verify the validation of the proposed method. Coolant channel milling experiments were conducted on a dual-spindle machine tools. For a nozzle with machining area about 8 m^2, the correlative accuracy achieved ±0.1 mm.

(IV) Sometimes, the two deformations appear simultaneously, including the stress-induced monolithic deformation and force-induced local deformation should be concerned simultaneously. Thus, how to compensate the coupled deformation needs further development.

Acknowledgments This work is supported by Funding Agency National Basic Research Program of China (Grant No.2014CB046604), Funding Agency National Natural Science of China (Grant No. 51305062) and China Postdoctoral Science Foundation Grant (Grant No. 2013M540220).

References

1. Arnaud L, Gonzalo O, Seguy S, Jauregi H, Peigne G (2011) Simulation of low rigidity part machining applied to thin-walled structures. Int J Adv Manuf Technol 54:479–288
2. BudaK E, Altintas Y (1995) Modeling and avoidance of static form errors in peripheral milling of plates. Int J Mach Tools Manuf 35(3): 459–476
3. Chantzis D, Van-der-Veen S, Zettler J, Sim WM (2013) An industrial workflow to minimise part distortion for machining of large monolithic components in aerospace industry. Procedia CIRP 54(1):483–486

4. Chen W, Xue J, Tang D, Chen H, Qu S (2009) Deformation prediction and error compensation in multilayer milling processes for thin-walled parts. Int J Mach Tools Manuf 49:859–864
5. Cho MW, Seo T (2002) Inspection planning strategy for the on-machine measurement process based on CAD/CAM/CAI integration. Int J Adv Manuf Technol 19:607–617
6. Cho MW, Seo T, Kwon HD (2003) Integrated error compensation method using OMM system for profile milling operation. J Mater Process Technol 136:88–99
7. Ding H, Zhu LM (2011) Geometric theories and methods for digital manufacturing of complex surfaces. Science Press, Beijing
8. Guiassa R, Mayer JRR (2011) Predictive compliance based model for compensation in multi-pass milling by on-machine probing. CIRP Ann Manuf Technol 60(1):391–394
9. Guiassa R, Mayer JRR, Balazinski M, Engin S, Delorme FE (2014) Closed door machining error compensation of complex surfaces using the cutting compliance coefficient and on-machine measurement for a milling process. Int J Comput Integr Manuf 27(11): 1022–1030
10. Guo D (2011) Function-geometry integrated precision machining methods and technologies for high performance workpieces. Chin Eng Sci 13(10):47–57
11. Huang N, Bi Q, Wang Y, Sun C (2014) 5-Axis adaptive flank milling of flexible thin-walled parts based on the on-machine measurement. Int J Mach Tools Manuf 8:1–8
12. Jia ZY, Ji T, Guo DM, Bian GH (2004) A precision grinding technique for radome inner surfaces. Key Eng Mater 257–258:177–182
13. Kim SH, Ko TJ, Ahn JH (2002) Elimination of settling error due to clamping forces in on-machine measurement. Int J Adv Manuf Technol 19:573–578
14. Kondo K, Hasegawa K, Kawamata H, Morishita T, Naito F (2012) On-machine non-contact dimension-measurement system with laser displacement sensor for vane-tip machining of RFQs. Nucl Instrum Methods Phys Res Sect A 667:5–10
15. Liu HB, Wang YQ, Huang XP, Xue L (2013) Isoplanar-based adaptive sampling for model-unknown sculptured surface coordinate metrology using non-contact probe. Int J Adv Manuf Technol 64: 1695–1707
16. Marusich TD, Usui S, Lankalapalli S, Saini N, Zamorano L, Grevstad A (2006) Residual stress prediction for part distortion modeling. SAE, 2006, 2006-01-3171
17. Mears L, Roth JT, Djurdjanovic D, Yang XP, Kurfess T (2009) Quality and inspection of machining operations–CMM integration to the machine tool. J Manuf Sci Eng-Trans ASME 131: 051006(1-13)
18. Rai JK, Xirouchakis P (2008) Finite element method based machining simulation environment for analyzing part errors induced during milling of thin-walled components. Int J Mach Tools Manuf 48(6): 629–643
19. Ratchev S, Liu S, Huang W, Becker AA (2006) An advanced FEA based force induced error compensation strategy in milling. Int J Mach Tools Manuf 46:542–551
20. Smith KS, Woody BA (2005) Improving the accuracy of large scale monolithic parts using fiducials. CIRP Ann Manuf Technol 54(1): 483–486
21. Smith S, Wilhelm R, Dutterer B, Cherukuri H, Goel G (2012) Sacrificial structure preforms for thin part machining. CIRP Ann Manuf Technol 61(1):379–382
22. Soroush M, Saeid A, Ehsan S, Hamdollah EC (2015) Effect of machining-induced residual stress on the distortionof thin-walled parts. Int J Adv Manuf Technol 76:597–608
23. Uriarte L, Zatarain M, Axinte D, Yague-Fabra J, Ihlenfeldt S, Eguia J, Olarra A (2013) Machine tools for large parts. CIRP Ann Manuf Technol 62(2):731–750
24. Wei Y, Wang XW (2007) Computer simulation and experimental study of machining deflection due to original residual stress of aerospace thin-walled parts. Int J Adv Manuf Technol 33:260–265
25. Woody BA, Smith KS, Hocken RJ, Miller JA (2007) A technique for enhancing machine tool accuracy by transferring the metrology reference from the machine tool to the workpiece. J Manuf Sci Eng Trans ASME 129(3):636–643